

GUIDANCE BREAKS THE FITTED OPERATOR: A TERMINAL-FITTED REPAIR FOR CLASSIFIER-FREE GUIDANCE

Shiheng Zhang
University of Washington
shzhang3@uw.edu

ABSTRACT

Classifier-free guidance (CFG) is the standard way to strengthen class-conditioning in diffusion and flow-matching samplers, yet at large guidance it oversaturates and destabilizes—symptoms practitioners suppress with more steps or limited-interval schedules. We analyze CFG through an asymptotic-preserving, numerical-analysis lens. Building on a recent result [12] that the deterministic DDIM step is the unique *fitted* operator for the unguided terminal layer—exact on the final, small- σ stretch of sampling—we show that guidance re-stiffens *exactly* the discriminative subspace to an anomalous exponent $1 + w$ (guided coordinates contract like σ^{1+w} rather than σ). DDIM is therefore no longer fitted there, and on coarse meshes its guided residual diverges as $\sigma_{\min} \rightarrow 0$. We prove a guided clock barrier with three ordered step-size thresholds, and read one-step oversaturation as its endpoint—a solver artifact on the calibration model rather than the continuous guided law. The same analysis yields a one-coefficient, zero-extra-NFE repair: replace CFG’s $w(r - 1)$ by $r^{1+w} - r$ on the guidance direction. This coefficient is the unique spectrum-free terminal-exact one, and it preserves the sign of every analyzed coordinate. On the calibration model’s discriminative crossover it removes CFG’s σ_{\min} -divergent blow-up and is first-order accurate against the exact guided flow as $\sigma_{\min} \rightarrow 0$ —asymptotic-preserving in σ_{\min} , though not uniform in w . On learned CIFAR-10 checkpoints—and, as a cross-domain smoke test, on Stable Diffusion 1.5 DDIM—it acts as a high-guidance stabilizer at no extra cost rather than a universal quality knob: it cuts residual amplification and saturation and gives 9/9 point-FID wins over CFG on the tested grid, while in the hard-cell blocks its classifier-proxy target accuracy stays close to CFG and terminal guidance shutdown loses much more. We report the limits alongside: it is not a universal image-quality win (KID can favor CFG; an interval can win FID in some cells), and against a dense vanilla-CFG reference it is not a uniformly better integrator of that field.

1 INTRODUCTION

Diffusion and flow-matching samplers integrate a probability-flow ODE whose velocity field stiffens as the noise scale $\sigma \rightarrow \sigma_{\min}$: on a coordinate normal to the data manifold the exact flow contracts at exponent one, by σ_{n+1}/σ_n per step. A recent fitted-operator analysis of unguided samplers [12] shows that this terminal layer admits a *unique* fitted (layer-exact) one-step operator: a frozen-field Euler step—Euler with the velocity held at its start-of-step value—reproduces that exact contraction if and only if its integration variable is affine in σ . This singles out the σ -clock step, algebraically identical to deterministic DDIM [11], and makes it *asymptotic-preserving* (AP) on the exactly solvable calibration models studied there [12]—uniformly accurate as $\sigma_{\min} \rightarrow 0$. This paper asks one question of that lens: *what survives of DDIM’s fitted-operator protection once we turn on guidance?*

Guidance re-stiffens the discriminative subspace. Classifier-free guidance (CFG) [7] runs the sampler on an extrapolated denoiser $D_w = (1 + w)D_c - wD_u$, that is, on a second velocity field $\eta_w = \eta_c + w(\eta_c - \eta_u)$ (the η ’s are noise-prediction fields; Section 2) with guidance scale $g =$

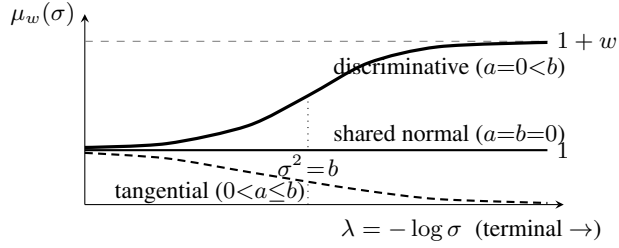


Figure 1: The guided terminal exponent $\mu_w(\sigma)$ by layer type on the commuting model (schematic; noise decreases to the right). Guidance leaves the shared-normal exponent at one and freezes tangential directions, but re-stiffens the discriminative directions to $1 + w$ —the subspace on which DDIM+CFG exits the class of fitted operators. Here a, b are the class and marginal variances along the direction (Section 2).

$1 + w$. This is not a uniform stiffening. On the commuting Gaussian model of Section 2, the guided terminal exponent $\mu_w(\sigma)$ splits by layer (a *layer* here is a regime of state-space directions, not a network layer; Figure 1): it stays exactly one on directions shared by the class and the marginal, freezes to zero on tangential directions, and rises to $1 + w$ on the *discriminative* directions—the subspace that separates the class from the marginal (Proposition 1). Guidance re-stiffens precisely this discriminative subspace, and it does so with a *second* singular parameter: w enters the terminal structure on the same footing as σ_{\min} . Because D_w is not any distribution’s posterior mean, DDIM’s fitted-operator protection lapses there: on coarse meshes, vanilla DDIM+CFG leaves the class of fitted operators and its terminal residual diverges as $\sigma_{\min} \rightarrow 0$.

Two orthogonal bills. This is a statement about the *solver*. A parallel line studies how the continuous guided law itself departs from the tilted conditional it is meant to sample [1, 2]: that charges the *model*; we charge the *discretization*—our reference solution is always the exact guided flow’s own pushforward. The two bills are orthogonal, and conflating them has obscured how much of guidance’s terminal pathology—the oversaturation and norm inflation seen at large w [10]—has a solver-induced component that appears even when the exact guided flow is the reference, from stepping guidance with an operator it has quietly un-fitted.

The repair is one coefficient. Rectifying the anomalous exponent $1 + w$ by a gauge change and pushing the σ -clock step through it yields a one-coefficient modification of CFG that touches nothing else in the sampler—only the coefficient on the guidance direction $D_u - D_c$ changes:

$$\begin{aligned} \text{CFG: } x_{n+1} &= D_c + r(x_n - D_c) + w(r - 1)(D_u - D_c), \\ \text{fitted: } x_{n+1} &= D_c + r(x_n - D_c) + (r^{1+w} - r)(D_u - D_c), \end{aligned}$$

with $r = \sigma_{n+1}/\sigma_n$. It uses the same two denoiser evaluations per step—the implementation delta is a single line, at zero additional NFE (network function evaluations)—agrees with CFG to first order, and reduces to DDIM at $w = 0$. We call it the guided fitted step, or *fitted CFG*. It is the *unique* scalar coefficient that is exact on the discriminative terminal layer using no spectral information (Lemma 2); it never reflects a coordinate across the class manifold (Proposition 3); and its one-step $r \rightarrow 0$ limit lands on the conditional denoiser D_c (the terminal-limit class projection), where vanilla CFG lands on the overshoot D_w , the discrete mechanism of oversaturation.

Contributions.

- **Structure and a barrier.** A layer classification of the guided terminal exponent (Proposition 1) and a guided clock barrier (Theorem 1) with three ordered step-size thresholds—reflection, residual-amplification failure (Section 3), absolute stability—and the resulting two-tier guidance tax on step count (Corollary 1).
- **Oversaturation as an endpoint, and the guidance interval.** A model-free identity reading one-step DDIM+CFG’s overshoot to D_w as the barrier’s $r \rightarrow 0$ endpoint (Remark 2), and a parameter-free prediction of the *terminal* edge of limited-interval guidance [9] (Remark 3).

- **A spectrum-free fitted repair.** The guided fitted step (Definition 1): first-order consistent, sign-preserving and terminal-exact on the model, unique (Lemma 2), and—on the discriminative crossover—free of the σ_{\min} -divergent blow-up and first-order accurate as $\sigma_{\min} \rightarrow 0$ (Proposition 4, Theorem 2): asymptotic-preserving in σ_{\min} , though not uniform in w .
- **A scoped empirical program.** On learned CIFAR-10 EDM [8] checkpoints, fitted CFG is a zero-extra-NFE high-guidance stabilizer: the residual and clipping certificates improve in both $w \in \{6.5, 8\}$ cells; the hard-cell image evaluations (two 5k blocks, a 50k replication) give it the best FID with target accuracy preserved, and a DINOv2 backbone-swap keeps the same fitted-favoring ordering; a nine-cell grid gives 9/9 FID wins over CFG. We report the limits alongside—the CFG-favoring KID split and threshold-derived interval baselines that win FID/KID at lower conditionality (Section 4).

Section 6 collects the claim boundaries.

2 THE GUIDED FLOW AND ITS TERMINAL LAYERS

The unguided flow. We work throughout in the variance-exploding family: $p_\sigma = p_{\text{data}} * \mathcal{N}(0, \sigma^2 I)$ for $\sigma \in [\sigma_{\min}, \sigma_{\max}]$, with denoiser $D(x, \sigma) = \mathbb{E}[x_0 \mid x_\sigma = x]$ and normalized residual $\eta = (x - D)/\sigma$ —the noise prediction $\hat{\varepsilon}$ of practice ($-\sigma \nabla_x \log p_\sigma$); not DDIM’s stochasticity parameter, which is 0 throughout. The probability flow ODE is $dX/d\sigma = \eta(X, \sigma)$, and the decomposition $x = D + \sigma\eta$ splits the state into a slow manifold component and a stiff normal component—normal to the data manifold, contracting fastest—whose exponent is 1: on a normal coordinate the exact flow contracts by $(\sigma_{n+1}/\sigma_n)^1$ per step. A fitted-operator analysis of the unguided terminal layer [12] shows that a frozen-field Euler step is layer-exact if and only if its clock is affine in σ , making the σ -clock step—algebraically the deterministic DDIM update [11]—the unique fitted operator up to affine reparameterization, with rectified flow its flow-matching counterpart; this fitted-operator property is what makes it asymptotic-preserving as $\sigma_{\min} \rightarrow 0$. The present paper asks what survives of that protection under guidance.

Guidance as a second velocity field. Classifier-free guidance [7] replaces the conditional denoiser $D_c(x, \sigma)$ by the extrapolation

$$D_w = (1 + w) D_c - w D_u, \quad w \geq 0, \quad (1)$$

where D_u is the unconditional (marginal) denoiser and $g = 1 + w$ is the guidance scale of practice, so $w = 6.5$ is CFG scale $g = 7.5$. Writing $\eta_c = (x - D_c)/\sigma$ and $\eta_u = (x - D_u)/\sigma$, the sampled dynamics is the *guided flow*

$$\frac{dX}{d\sigma} = \eta_w = (1 + w) \eta_c - w \eta_u = \eta_c + w \gamma, \quad \gamma := \eta_c - \eta_u = \frac{D_u - D_c}{\sigma}, \quad (2)$$

with γ the normalized guidance direction. Equation (2) is the dynamical statement of guidance: the sampler follows the conditional velocity plus w times the discriminative correction. Two facts follow. First, D_w is in general not a VE posterior mean with a positive-semidefinite Tweedie covariance, so η_w is not the residual of such a denoiser; the rigidity theorem that singles out DDIM as layer-exact inside the unguided denoiser class [12] no longer applies directly. The exit is quantitative, not merely definitional: for any true denoiser, $J_D = \nabla_x D = \text{Cov}(X_0 \mid x)/\sigma^2 \succeq 0$ [4] caps the exponent of the residual field at 1 (on the model, the residual exponent is $A \leq 1$ in (3)), while on discriminative directions the guided exponent exceeds 1 at every σ (Proposition 1)—no repackaging of any denoiser, affine or otherwise, reproduces the guided field. Second, the guided flow carries a *second* parameter: any AP statement must state its w -dependence, and the fitted step below removes the σ_{\min} -divergent terminal barrier for bounded w , though not uniformly in w .

The model problem. Our analysis is carried out on the guided analog of the unguided model problem [12].

Hypothesis 1 (commuting class–marginal pair). $p_c = \mathcal{N}(0, C_c)$ and $p_u = \mathcal{N}(0, C_u)$ with $[C_c, C_u] = 0$, and on the shared eigenbasis the spectra satisfy $a_i \leq b_i$.

The ordering $a_i \leq b_i$ is the *class-subset hypothesis*: the class is narrower than the marginal in every probed direction (as when the marginal is a mixture whose components share the class covariance).

Real learned checkpoints need not obey it; the reverse case is a genuine model boundary, discussed in Remark 4. On an eigen-coordinate ξ with class variance a and marginal variance b , the two denoisers are linear and the residuals are

$$\eta_c = A \frac{\xi}{\sigma}, \quad \eta_u = B \frac{\xi}{\sigma}, \quad A := \frac{\sigma^2}{a + \sigma^2}, \quad B := \frac{\sigma^2}{b + \sigma^2}, \quad 0 \leq B \leq A \leq 1. \quad (3)$$

The guided flow (2) therefore closes coordinate-wise,

$$\frac{d \log \xi}{d \log \sigma} = \mu_w(\sigma) := (1+w)A - wB = A + w(A-B), \quad (4)$$

and every question about clocks, stability, and fitted operators reduces to the behavior of the *exponent function* μ_w .

Proposition 1 (layer classification under guidance). *Under Hypothesis 1, as $\sigma \rightarrow 0$ the exponent function (4) satisfies: (i) on shared normal directions ($a = b = 0$), $\mu_w \equiv 1$: the guidance weight cancels and the layer is the unguided exponent-1 layer; (ii) on tangential directions ($0 < a \leq b$), $\mu_w \rightarrow 0$: the coordinate freezes; (iii) on discriminative normal directions ($a = 0 < b$),*

$$\mu_w(\sigma) = 1 + w \frac{b}{b + \sigma^2} \rightarrow 1 + w, \quad (5)$$

monotonically as σ decreases, with crossover midpoint at $\sigma^2 = b$.

(Proofs for Sections 2 and 3 are deferred to Appendix A.)

Proposition 1 is the structural fact of the paper. Guidance does not stiffen the flow uniformly; it re-stiffens *exactly the discriminative subspace*—the directions collapsed within the class but present in the marginal ($a = 0 < b$)—and (5) locates where the re-stiffening begins: the anomalous exponent switches on as σ descends through the class-separation scale \sqrt{b} . Above that scale the guided flow is, to leading order, the unguided flow; below it, the terminal layer runs at exponent $1 + w$, and w enters the singular structure of the problem on the same footing as σ_{\min} .

Lemma 1 (exact guided factor). *Under Hypothesis 1, the exact solution of (2) on an eigen-coordinate over one step $\sigma_n \rightarrow \sigma_{n+1}$ is $\xi_{n+1} = \Phi_w \xi_n$ with*

$$\Phi_w = \left(\frac{a + \sigma_{n+1}^2}{a + \sigma_n^2} \right)^{\frac{1+w}{2}} \left(\frac{b + \sigma_n^2}{b + \sigma_{n+1}^2} \right)^{\frac{w}{2}}. \quad (6)$$

In particular, on a discriminative coordinate ($a = 0$), writing $r = \sigma_{n+1}/\sigma_n$,

$$\Phi_w = r^{1+w} \left(\frac{b + \sigma_n^2}{b + \sigma_{n+1}^2} \right)^{\frac{w}{2}}, \quad (7)$$

which tends to r^{1+w} once $\sigma_n^2 \ll b$.

The singular limit now has two knobs. As $\sigma_{\min} \rightarrow 0$ the discriminative layer contracts by the anomalous power σ^{1+w} ; as w grows at fixed σ_{\min} the same layer stiffens without bound. We ask two questions: which part of DDIM+CFG’s failure is the pure terminal-layer solver barrier, and can that barrier be removed by a one-coefficient fitted repair? Uniform accuracy through the finite- σ crossover is separate, needing either mesh resolution of the crossover or the spectrum-aware Gaussian factor.

3 THE GUIDED BARRIER AND THE FITTED OPERATOR

This section establishes one claim: *classifier-free guidance introduces a second singular parameter w , and on discriminative terminal directions the σ -clock frozen-field step—DDIM applied to the guided denoiser—is no longer fitted.* The program has three parts. First, a barrier: the guided analog of the unguided clock dichotomy [12], with sharp thresholds in the log-step h and weight w (Theorem 1). Second, an operator: a fitted step that removes the pure discriminative terminal-layer reflection and σ_{\min} -divergent residual blow-up at zero additional cost (Definition 1). Third, accuracy: a first-order certificate on the discriminative crossover (Theorem 2); the whole-model theory remains future work. Throughout, the reference solution is the exact guided flow’s own pushforward: we charge the *discretization* of (2), not the distortion of the continuous guided law away from the tilted conditional (Section 1).

The frozen step. DDIM applied to D_w —equivalently, σ -clock Euler with the guided field frozen at the left endpoint—is

$$x_{n+1} = x_n + (\sigma_{n+1} - \sigma_n) \eta_w(x_n, \sigma_n), \quad (8)$$

which on an eigen-coordinate of the model contracts by

$$G_{\text{CFG}} = 1 - (1 - r)[(1 + w)A - wB], \quad r = \frac{\sigma_{n+1}}{\sigma_n} = e^{-h}. \quad (9)$$

On the pure discriminative layer $(A, B) = (1, 0)$ this is

$$G_w(h) = 1 - (1 + w)(1 - e^{-h}) = (1 + w)e^{-h} - w, \quad (10)$$

to be compared with the exact factor $e^{-(1+w)h}$ of Lemma 1. Here $h = \log(\sigma_n/\sigma_{n+1})$ is the step in $\lambda = -\log \sigma$ (half the VE log-SNR), so a uniform λ -mesh has constant h . Along a trajectory, call $\max_n \|\eta_w(x_n, \sigma_n)\|/\|\eta_w(x_0, \sigma_0)\|$ the *residual-amplification certificate*, written amp; the sampler already forms every quantity in it, and a scheme is residual-stable if the certificate stays bounded as $\sigma_{\min} \rightarrow 0$. Everything in Theorem 1 is a statement about the elementary function (10).

Theorem 1 (guided clock barrier). *Consider the frozen step (8) on the pure discriminative layer, $\eta_w = (1 + w)\xi/\sigma$ with $w > 0$, on a uniform λ -mesh of step h . Let*

$$h_b = \log\left(1 + \frac{1}{w}\right), \quad h_{\#} = \log\left(1 + \frac{2}{w}\right), \quad h_{\infty} = \log\left(\frac{1+w}{w-1}\right) \quad (w > 1). \quad (11)$$

Then $h_b < h_{\#} < h_{\infty}$, and:

- (a) **Sign.** $G_w(h) > 0$ iff $h < h_b$; equivalently, at fixed h , sign preservation fails once $w > 1/(e^h - 1)$. For $h > h_b$ every step reflects the coordinate across the class manifold.
- (b) **Residual amplification.** The per-step residual amplification is $|G_w(h)|e^h$, which is ≤ 1 iff $h \leq h_{\#}$; equivalently, raw amplification begins once $w > 2/(e^h - 1)$. For $h > h_{\#}$ the amplification factor is $we^h - (1 + w) > 1$ per step. On a terminal subwindow $\sigma \in [\sigma_{\min}, \varepsilon\sqrt{b}]$, where $B \leq \varepsilon^2/(1 + \varepsilon^2)$ makes the exact per-step factor pure-layer up to $O(\varepsilon^2)$, of λ -length $\Lambda_{\varepsilon} = \log(\varepsilon\sqrt{b}/\sigma_{\min})$ the guided residual grows by

$$(we^h - (1 + w))^{\Lambda_{\varepsilon}/h} = \left(\frac{\varepsilon\sqrt{b}}{\sigma_{\min}}\right)^{\rho}, \quad \rho = \frac{\log(we^h - (1 + w))}{h} > 0, \quad (12)$$

so for fixed $\varepsilon > 0$ and $h > h_{\#}$ the scheme fails the amplification certificate as $\sigma_{\min} \rightarrow 0$.

- (c) **Absolute stability.** $|G_w(h)| \leq 1$ for all h when $w \leq 1$; for $w > 1$, iff $h \leq h_{\infty}$.

All three thresholds decay like c/w as $w \rightarrow \infty$, with $c = 1, 2, 2$ respectively.

In words: sign preservation fails first (a, above h_b : every step reflects across the class manifold), the certificate second (b, above $h_{\#}$: the residual compounds, diverging as $\sigma_{\min} \rightarrow 0$), absolute stability last (c, only for $w > 1$).

Corollary 1 (two-tier guidance tax). *On a uniform λ -mesh covering the discriminative window (of λ -length $\Lambda_b = \log(\sqrt{b}/\sigma_{\min})$), avoiding reflection requires*

$$N \geq \frac{\Lambda_b}{\log(1 + 1/w)} \sim w \Lambda_b, \quad (13)$$

while merely keeping the residual nonexpansive requires $N \geq \Lambda_b/\log(1 + 2/w) \sim \frac{w}{2} \Lambda_b$. A uniform global mesh must meet this bound throughout the window, so Λ_b is replaced by the full horizon $\Lambda = \log(\sigma_{\max}/\sigma_{\min})$: at working scale $g = 7.5$ ($\Lambda = \log(80/0.002) \approx 10.6$), reflection-free sampling already demands $N \gtrsim 74$ steps—an order of magnitude above unguided-DDIM-accurate budgets [8].

Remark 1 (the reflecting window). In the window $h \in (h_b, h_{\#}]$ the scheme is *reflecting but non-expansive*: the flip does not grow the residual. The flip is the mechanism of visible artifacts—the iterate lands on the wrong side of the class manifold each step—while the amplification crossing at $h_{\#}$ is where the certificate, and any uniform accuracy claim, actually fails. Practitioners tune w down at low σ well before the certificate diverges: part (a), not part (b), is the threshold their tuning discovers.

Remark 2 (the one-jump limit is oversaturation). The following identity is model-free. A single frozen step (8) from σ_n to $\sigma_{n+1} = r\sigma_n$ with $r \rightarrow 0$ gives

$$x_{n+1} \rightarrow x_n - \sigma_n \eta_w(x_n, \sigma_n) = (1+w)D_c - wD_u = D_w(x_n, \sigma_n): \quad (14)$$

one-step DDIM+CFG lands on the *extrapolated* denoiser, displaced from the class manifold by $-w(D_u - D_c)$. On the model this is the reflection $\xi \mapsto -w\xi$ of Theorem 1(a) pushed to its endpoint. We read this as the discrete mechanism of the oversaturation and norm-inflation phenomenology reported for large guidance scales [10]: it is a property of the *solver* at coarse steps, not of the continuous guided flow—on the calibration model the exact flow contracts to D_c as r^{1+w} while the frozen step overshoots to D_w .

The guided fitted step. The repair is dictated by the same logic that produced DDIM in the unguided setting [12]: integrate the stiff layer exactly and freeze what is slow. The gauge $\tilde{\xi} = \sigma^{-w}\xi$ rectifies the anomalous exponent $1+w$ to exponent 1; transporting the σ -clock Euler step through the gauge and back yields, on the whole state,

Definition 1 (guided fitted step). With $r = \sigma_{n+1}/\sigma_n$ and all fields evaluated at (x_n, σ_n) ,

$$x_{n+1} = D_c + r(x_n - D_c) + (r^{1+w} - r)(D_u - D_c). \quad (15)$$

equivalently, in residual form,

$$x_{n+1} = x_n + (\sigma_{n+1} - \sigma_n)\eta_c + \sigma_n(r^{1+w} - r)\gamma. \quad (16)$$

The scheme touches exactly one coefficient of classifier-free guidance: vanilla DDIM+CFG is (15) with the coefficient $w(r-1)$ in place of $r^{1+w} - r$ on the guidance direction $D_u - D_c$. It uses the same two denoiser evaluations per step, so the cost—and the implementation delta—is one line. Proposition 3 verifies the factor coordinate-wise; Lemma 2 pins the coefficient from terminal exactness alone.

Proposition 2 (consistency). $r^{1+w} - r = w(r-1) + \frac{1}{2}w(w+1)h^2 + O(h^3)$ as $h \rightarrow 0$, so (15) is a first-order-consistent discretization of the guided flow (2), agreeing with DDIM+CFG through $O(h)$; and at $w = 0$ both coefficients vanish identically, collapsing the scheme to DDIM.

Proposition 3 (the fitted step is sign-preserving and terminal-exact). Under Hypothesis 1, the step (15) contracts an eigen-coordinate by

$$G_{\text{fit}} = 1 - (1-r)A + (r^{1+w} - r)(A - B) = (1-A) + rB + r^{1+w}(A - B), \quad (17)$$

a sum of nonnegative terms; hence $G_{\text{fit}} > 0$ on every coordinate, for every mesh, and every $w \geq 0$: the fitted step preserves the sign of every analyzed coordinate. It is exact in the three terminal regimes— $G_{\text{fit}} = r$ on shared normals ($A = B = 1$), $G_{\text{fit}} = r^{1+w}$ on pure discriminative normals ($A = 1, B = 0$), and $G_{\text{fit}} = 1$ on frozen tangential directions ($A = B = 0$)—and its one-jump limit is $x_{n+1} \rightarrow D_c$, the conditional denoiser (the terminal-limit class projection), in contrast with (14).

Lemma 2 (uniqueness of the scalar terminal coefficient). Consider scalar coefficient updates of the form

$$x_{n+1} = D_c + r(x_n - D_c) + \alpha(r, w)(D_u - D_c),$$

where α depends only on (r, w) . The unique such coefficient that is exact on the pure discriminative terminal regime $(A, B) = (1, 0)$ is

$$\alpha(r, w) = r^{1+w} - r.$$

Consequently, terminal exactness, DDIM recovery at $w = 0$, and exactness on the shared-normal and tangent terminal regimes determine the fitted coefficient without any spectrum information.

Proposition 4 (finite crossover tax for the fitted step). On a single discriminative Gaussian coordinate with $a = 0 < b$, define

$$q(\sigma) = 1 - B(\sigma) = \frac{b}{b + \sigma^2}, \quad \mu(\sigma) = \mu_w(\sigma) = 1 + wq(\sigma).$$

Let $\sigma_0 > \sigma_1 > \dots > \sigma_K$ be any decreasing mesh, $r_n = \sigma_{n+1}/\sigma_n$, $q_n = q(\sigma_n)$, and $\mu_n = \mu(\sigma_n)$. For the fitted step (15), the guided residual ratio over one step is

$$\frac{|\eta_w(\xi_{n+1}, \sigma_{n+1})|}{|\eta_w(\xi_n, \sigma_n)|} = \frac{\mu_{n+1}}{\mu_n} [(1 - q_n) + r_n^w q_n]. \quad (18)$$

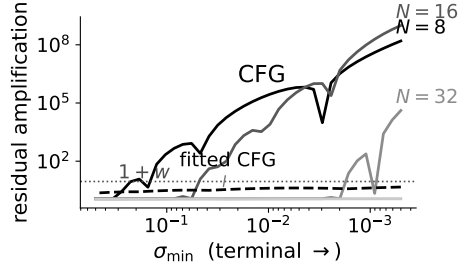


Figure 2: Synthetic crossover at $w = 8$: residual amplification as $\sigma_{\min} \rightarrow 0$. CFG develops the σ_{\min} -divergent branch of Theorem 1(b) on coarse meshes ($N \in \{8, 16, 32\}$), stabilizing only once $h < h_{\#}$ —the flat gray curve ($N=64$) coincides with the exact flow. The fitted step (dashed) stays below the $1 + w$ tax on every mesh.

Hence for every prefix k ,

$$\frac{|\eta_w(\xi_k, \sigma_k)|}{|\eta_w(\xi_0, \sigma_0)|} \leq \frac{\mu_k}{\mu_0} \leq 1 + w. \quad (19)$$

Thus the fitted step removes the σ_{\min} -divergent terminal blow-up of Theorem 1 on the discriminative crossover, but it may still pay a finite $O(1 + w)$ crossover tax on a coarse mesh.

Bounded amplification in fact upgrades to accuracy: on this crossover the accumulated log-defect (uniform mesh, $h \leq 1$) obeys $0 \leq \log \Theta_K \leq \frac{1+h}{4} w(w+2)h$, so the fitted step is *first-order uniformly accurate* against the exact guided flow’s own pushforward, with a W_2 bound whose constant is independent of b , K , and σ_{\min} (the $O(w^2)$ factor is not uniform in w). We defer the formal statement and proof to Theorem 2 in Appendix A.

Extending this crossover accuracy to the tangential layers and learned geometry needs the spectrum-aware Gaussian factor (6) and is future work.

Remark 3 (the terminal side of the guidance interval). Limited-interval guidance [9] disables guidance outside a tuned band $(\sigma_{\text{lo}}, \sigma_{\text{hi}})$ and leaves open whether the band can be derived rather than tuned. Theorem 1 supplies the terminal side without free parameters: on schedules whose local step h_n grows toward low σ (e.g. Karras power meshes; on a uniform λ -mesh h_n is constant and there is no distinct crossing), the level at which h_n crosses $h_b(w) = \log(1 + 1/w)$ predicts σ_{lo} : below it, frozen-field guidance at weight w is unaffordable and the interval or the fitted step must take over. The *high-noise* cutoff σ_{hi} is not explained by the barrier: there $\|D_u - D_c\|$ is small against the model’s own error, a signal-level criterion outside this paper’s ledger.

Remark 4 (the reverse ordering). If a direction has $b = 0 < a$, the exponent (4) tends to $-w$: the *continuous* guided flow expands as $\sigma \rightarrow 0$, an instability of the guidance target that no solver can repair; the class-subset hypothesis excludes it by assumption (Appendix B).

Certificates. The certificate is removal of the σ_{\min} -divergent pure-layer mechanism (Proposition 4) plus first-order accuracy on the discriminative crossover (Theorem 2), not global residual nonexpansion through every finite- σ crossover.

4 EMPIRICAL DIAGNOSTICS ON LEARNED CHECKPOINTS

Synthetic crossover. Our primary residual and image-quality comparisons fix their schemes, cells, and metrics before each run; the feature-space, latent-diffusion, and dense-reference results are exploratory diagnostics. The single-coordinate Gaussian diagnostic isolates the theorem’s singular mechanism: on uniform log- σ meshes with $a = 0 < b$, CFG develops the coarse-mesh branch of Theorem 1 while the fitted coefficient stays below Proposition 4’s finite-tax bound (Figure 2). In the default w - N sweep, worst-case amplification reaches 10^3 – 10^9 for CFG but stays ≤ 4.66 for the fitted step, below each $1 + w$ bound—a theorem figure, not a learned-checkpoint quality metric.

Real-checkpoint residual diagnostics. We then test the coefficient as a drop-in replacement on NVIDIA EDM CIFAR-10 VP checkpoints [8] (the ‘VP’ label is network preconditioning only; sam-

Table 1: Real-checkpoint residual diagnostics. amp med and amp p95 (median and 95th-percentile residual amplification) are fitted-CFG/CFG ratios (< 1 means the repair shrinks it); clip Δ is fitted CFG minus CFG for the median fraction of final-denoised pixels outside $[-1,1]$.

w	N	class0			class1		
		amp med \downarrow	amp p95 \downarrow	clip Δ \downarrow	amp med \downarrow	amp p95 \downarrow	clip Δ \downarrow
4.0	8	0.993	0.867	-0.0236	0.997	0.985	-0.0177
4.0	16	1.001	0.878	-0.0225	1.001	1.012	-0.0360
4.0	32	1.013	0.871	-0.0231	1.002	1.012	-0.0529
6.5	8	0.695	0.149	-0.2889	0.666	0.132	-0.1421
6.5	16	0.821	0.534	-0.2926	0.933	0.659	-0.1978
6.5	32	0.836	0.512	-0.3120	0.971	0.668	-0.2231
8.0	8	0.309	0.128	-0.3786	0.203	0.116	-0.2306
8.0	16	0.668	0.132	-0.3937	0.593	0.129	-0.2876
8.0	32	0.544	0.216	-0.4271	0.704	0.288	-0.3853

Table 2: Image-quality evaluation at the hard cell $w=8, N=8$: two 5k seed blocks (A, B) and a 50k replication, for CFG, the fitted repair, and the terminal-interval baseline. FID/KID are feature-space quality metrics; amp p95 and clip p95 are the 95th-percentile residual amplification and final-denoise clipping fraction (per scheme, not a ratio); target acc is classifier target-label accuracy (%). **Bold** marks the per-block best of the two feature metrics: fitted CFG wins FID everywhere, CFG wins KID everywhere.

	scheme	FID \downarrow	KID \downarrow	amp p95 \downarrow	clip p95 \downarrow	target acc \uparrow
5k (A)	CFG	32.44	0.0110	13.32	0.570	94.96
	fitted	25.22	0.0181	1.66	0	94.66
	interval	26.46	0.0224	1.63	0	89.24
5k (B)	CFG	31.98	0.0107	13.20	0.572	94.88
	fitted	24.89	0.0173	1.64	0	94.34
	interval	26.04	0.0211	1.62	0	90.00
50k	CFG	27.86	0.0108	13.34	0.569	95.14
	fitted	20.88	0.0177	1.65	0	94.83
	interval	22.08	0.0221	1.63	0	88.95

pling uses the σ -parameterization): D_c is the class-conditional checkpoint, D_u the separately trained unconditional one, and both schemes use the same Karras mesh, seeds, labels, and NFE. The grid is $w \in \{4, 6.5, 8\}$ and $N \in \{8, 16, 32\}$, with two 64-seed blocks (class 0, seeds from 1000; class 1, from 2000). Table 1 reports paired fitted/CFG ratios for the amplification median and tail, and paired clipping differences; lower is better.

In both blocks, for every tested $N \in \{8, 16, 32\}$ at $w = 6.5$ and $w = 8$, fitted CFG improves the amp median, amp p95, and clipping median. The hardest cell is the clearest: at $w = 8, N = 8$, the class-0 amp median/p95 falls from 4.57/13.35 under CFG to 1.41/1.71 under fitted CFG, while the clipping median drops from 0.379 to 0; the class-1 replicate matches (amp p95 ratio 0.116, clipping delta -0.23). At $w = 4$, where the theory predicts a much weaker tax, the median amplification is mixed, but the amp tail and saturation proxy still improve in most cells. We use this as evidence for high-guidance stabilization, not uniform superiority at weak guidance.

Image-quality evaluation. We next ran two 5000-image balanced-class evaluations on the hard cell $w = 8, N = 8$, plus a 50k replication, each including a terminal-interval baseline (vanilla CFG correction off when $h > h_b$, after Kynkäänniemi et al. [9]; on this coarse mesh every step crosses h_b , so it reduces to unguided conditional DDIM). We score with FID and KID (feature-space quality metrics; lower is better). Table 2 collects the results. Fitted CFG has the best FID in all three blocks at zero extra NFE, and the certificates replicate (amp p95 falls from 13+ to ≈ 1.6 , clipping p95 from ≈ 0.57 to 0). The metrics disagree, however: KID is lowest for CFG in every block. We therefore read this as support for high-guidance stabilization and FID improvement, not an unqualified image-quality win; feature-manifold and sharpness diagnostics are consistent with CFG’s oversaturation contributing to the split (Figure 3), and a DINOv2 backbone-swapped audit gives the same fitted-favoring ordering, so the split is not Inception-specific (Appendices C and D).

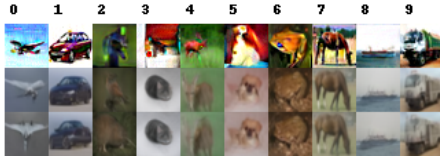


Figure 3: Uncurated hard-cell samples ($w=8$, $N=8$; first ten CIFAR-10 classes, matched seeds). Rows: CFG, fitted CFG, terminal-interval. CFG’s row is visibly more saturated and higher-contrast; the repair and interval are lower-contrast at zero extra NFE. Qualitative only—KID still favors CFG.

Finally, the target-accuracy column of Table 2 is a classifier-conditionality diagnostic (classifier at 94.37% on the CIFAR-10 test set): in every block fitted CFG stays within 0.6pp of CFG yet ~ 5 pp above interval, keeping CFG’s conditional pull without its clipping pathology.

Robustness grid. The 50k replication (Table 2) reduces the 5k-sampling-artifact concern for the FID ordering, and the KID split persists at scale. A nine-cell grid ($w \in \{4, 6.5, 8\}$, $N \in \{8, 16, 32\}$, 5k images each) shows it is not cell-specific: fitted CFG improves FID in 9/9 cells, clipping p95 in 9/9, and amp p95 in 8/9 (exception $w=4$, $N=32$, both near 1). The terminal-interval baseline wins FID at $N \in \{16, 32\}$ and KID at $N = 32$ but loses conditionality everywhere (3.24–5.72pp).

Interval-baseline separation. Is the fitted step just guidance shutdown? We compared it against a *tuned* conditionality-preserving limited interval (selected per cell) and the parameter-free terminal interval (Appendix E). In the tested cells, the tuned interval preserves target accuracy but does not beat the fitted step on FID; the terminal interval can win FID (e.g. 12.63 vs 17.12 at $w=8$, $N=16$) but drops target accuracy by 5–6pp. So the fitted step gives interval-like residual stabilization while keeping the guided update active—it is not explained away by turning guidance off.

All-class audit. Extending the residual diagnostic from two classes to all ten CIFAR-10 classes on the high-guidance cells (60 class–cell pairs), clipping/saturation is non-increased in 60/60 pairs and amp p95 improves in 54/60: global saturation robustness and near-global residual-tail improvement (Appendix G).

Latent-diffusion smoke. The mechanism is not specific to pixel-space CIFAR. On Stable Diffusion 1.5 DDIM at high guidance, the same coefficient sharply reduces pixel saturation (p95 $0.134 \rightarrow 0.009$ at guidance 12, over 256 images) while preserving CLIP image–text alignment ($0.320 \rightarrow 0.314$); terminal guidance shutdown reaches lower saturation but collapses CLIP to 0.271 (Appendix F). This is a cross-domain smoke test, not a Stable Diffusion benchmark.

5 RELATED WORK

The CFG-repair family is crowded, and methods differ mainly in their *mathematical object*: a manifold projection, a guidance-vector rescaling, an interval schedule, a dynamic weight, or—ours—a terminal fitted-operator coefficient. In brief: CFG++ [3] constrains the update to the data manifold; limited-interval guidance [9] switches guidance off outside a σ band (Remark 3 derives its terminal edge parameter-free); APG [10] down-weights the update’s parallel component; CFG-Zero* [5] optimizes the scale and zero-inits early steps; and C²FG [6] decays the weight in time. None derives the terminal-fitted coefficient $r^{1+w} - r$ from the guided exponent—where the barrier lives. An orthogonal line analyses what the *continuous* guided law samples—CFG is a predictor–corrector, not a sampler of its tilted target [1, 2]—the “model” bill complementary to ours.

6 DISCUSSION AND LIMITATIONS

What is proved. On the commuting class-subset Gaussian model, the barrier (Theorem 1) is sharp; the fitted step is consistent, sign-preserving, terminal-exact, pays only a finite $O(1 + w)$ crossover tax (Prop. 4), and is first-order accurate on the crossover (Theorem 2)—all about the *discretization* against the guided flow’s own pushforward, AP in σ_{\min} but not uniform in w .

What is evidence. On learned CIFAR-10 EDM checkpoints, fitted CFG is a drop-in, zero-extra-NFE high-guidance stabilizer: the certificates improve residual amplification and clipping across every $w \in \{6.5, 8\}$ cell; the hard-cell evaluations (5k twice, 50k once) give it the best FID with target accuracy preserved, and a DINOv2 backbone-swap the same ordering; the nine-cell grid gives 9/9 FID wins over CFG. It separates from tuned and terminal interval baselines (which either lose target accuracy or fail to beat it on FID), holds across all ten classes (60/60 saturation non-increase, 54/60 amp-tail), and transfers to Stable Diffusion 1.5 DDIM as a saturation-reducing coefficient that keeps CLIP alignment far better than guidance shutdown (Section 4, Appendices E–G).

What is neither. We do not claim (i) an unqualified image-quality win—KID stays lowest for CFG at 5k and 50k, a split tied to CFG’s oversaturation without proven causation; (ii) that CIFAR verifies the sharp threshold law—the learned diagnostics are only *consistent with* the model ordering; or (iii) a 50k KID win or many-cell large-sample result—the 50k run is one hard cell. Nor is the fitted step a uniformly better integrator of the vanilla CFG field on learned checkpoints: against a 512-step CFG reference its residual tails shrink but its final-image L_2 does not (Appendix H), an interval can win FID in some cells by weakening guidance, and the Stable Diffusion result is a smoke test, not a benchmark. The class-subset hypothesis is itself a boundary: where the class is *wider* than the marginal, the continuous guided flow is unstable (exponent $-w$), which no solver can repair (Remark 4).

Scope and outlook. Every certificate uses only sampler-computed quantities from two separate checkpoints, so shared-head correlations cannot inflate them. ‘Asymptotic-preserving’ is used in the calibration-model sense: on learned checkpoints we audit AP-relevant residuals rather than certify AP. Next: shared-dropout CFG, broader latent-diffusion benchmarks, and a whole-model accuracy theory.

REPRODUCIBILITY STATEMENT

All theoretical results are stated with explicit constants on the model of Hypothesis 1, and complete proofs appear in Appendix A. Every empirical diagnostic in Section 4 is produced by a self-contained script operating on the public NVIDIA EDM CIFAR-10 VP checkpoints with stated seeds, meshes, sample counts, schemes, and metrics; the synthetic-crossover and checkpoint-certificate scripts additionally ship CPU `--self-test` modes, and the synthetic crossover figure requires no checkpoints. The supplementary package contains the scripts, the exact commands, the run manifests, and all summary artifacts (CSV/JSON) behind every number reported in the paper, including the 50k and nine-cell grid diagnostics.

REFERENCES

- [1] Arwen Bradley and Preetum Nakkiran. Classifier-free guidance is a predictor-corrector. *Transactions on Machine Learning Research (TMLR)*, 2025. arXiv:2408.09000.
- [2] Muthu Chidambaram, Khashayar Gatmiry, Sitan Chen, Holden Lee, and Jianfeng Lu. What does guidance do? a fine-grained analysis in a simple setting. In *Advances in Neural Information Processing Systems (NeurIPS)*, 2024. arXiv:2409.13074.
- [3] Hyungjin Chung, Jeongsol Kim, Geon Yeong Park, Hyelin Nam, and Jong Chul Ye. CFG++: Manifold-constrained classifier free guidance for diffusion models. In *International Conference on Learning Representations (ICLR)*, 2025. arXiv:2406.08070.
- [4] Bradley Efron. Tweedie’s formula and selection bias. *Journal of the American Statistical Association*, 106(496):1602–1614, 2011.
- [5] Weichen Fan, Amber Yijia Zheng, Raymond A. Yeh, and Ziwei Liu. CFG-Zero*: Improved classifier-free guidance for flow matching models. *arXiv preprint arXiv:2503.18886*, 2025.
- [6] Jiayang Gao, Tianyi Zheng, Jiayang Zou, Fengxiang Yang, Shice Liu, Luyao Fan, Zheyu Zhang, Hao Zhang, Jinwei Chen, Peng-Tao Jiang, Bo Li, and Jia Wang. C²FG: Control classifier-free guidance via score discrepancy analysis. In *Proceedings of the IEEE/CVF*

Conference on Computer Vision and Pattern Recognition (CVPR), pp. 34398–34407, 2026. arXiv:2603.08155.

- [7] Jonathan Ho and Tim Salimans. Classifier-free diffusion guidance. *arXiv preprint arXiv:2207.12598*, 2022.
- [8] Tero Karras, Miika Aittala, Timo Aila, and Samuli Laine. Elucidating the design space of diffusion-based generative models. In *Advances in Neural Information Processing Systems (NeurIPS)*, 2022.
- [9] Tuomas Kynkäänniemi, Miika Aittala, Tero Karras, Samuli Laine, Timo Aila, and Jaakko Lehtinen. Applying guidance in a limited interval improves sample and distribution quality in diffusion models. In *Advances in Neural Information Processing Systems (NeurIPS)*, 2024. arXiv:2404.07724.
- [10] Seyedmorteza Sadat, Otmar Hilliges, and Romann M. Weber. Eliminating oversaturation and artifacts of high guidance scales in diffusion models. In *International Conference on Learning Representations (ICLR)*, 2025. arXiv:2410.02416.
- [11] Jiaming Song, Chenlin Meng, and Stefano Ermon. Denoising diffusion implicit models. In *International Conference on Learning Representations (ICLR)*, 2021.
- [12] Shiheng Zhang. Asymptotic-preserving a posteriori analysis of diffusion and flow-matching samplers. *arXiv preprint arXiv:2607.04113*, 2026.

A DEFERRED PROOFS

Proof of Proposition 1. For $a = 0$ one has $A \equiv 1$, so $\mu_w = (1 + w) - wB = 1 + w(1 - B) = 1 + wb/(b + \sigma^2)$; the limits and monotonicity are immediate. Cases (i) and (ii) follow from $A, B \rightarrow 1$ and $A, B \rightarrow 0$ respectively. \square

Proof of Lemma 1. Integrate (4): $\int \mu_w d \log \sigma = \frac{1+w}{2} \log(a + \sigma^2) - \frac{w}{2} \log(b + \sigma^2)$ up to a constant, since $d \log(c + \sigma^2) = 2A_c d \log \sigma$ with $A_c = \sigma^2/(c + \sigma^2)$. Exponentiate the increment. \square

Proof of Theorem 1. From (10): $G_w > 0 \iff e^{-h} > w/(1 + w) \iff h < \log(1 + 1/w)$, which is (a). For (b), on the pure layer $\eta_w \propto \xi/\sigma$, so the residual ratio per step is $|\xi_{n+1}/\xi_n| \cdot \sigma_n/\sigma_{n+1} = |G_w|e^h$. On the branch $G_w \leq 0$ this is $(w - (1 + w)e^{-h})e^h = we^h - (1 + w)$, which exceeds 1 iff $e^h > 1 + 2/w$; on the branch $G_w \geq 0$ it equals $(1 + w) - we^h \leq 1$ always. Compounding over Λ_ε/h steps gives (12). For (c), $G_w \leq 1$ always, and $G_w \geq -1 \iff (1 + w)e^{-h} \geq w - 1$, vacuous for $w \leq 1$ and equivalent to $h \leq h_\infty$ otherwise. The ordering $h_\# < h_\infty$ follows from $\frac{1+w}{w-1} - (1 + \frac{2}{w}) = \frac{2}{w(w-1)} > 0$. \square

Proof of Proposition 2. $r^{1+w} - r = e^{-(1+w)h} - e^{-h}$ and $w(r - 1) = w(e^{-h} - 1)$; both are $-wh + O(h^2)$, and expanding to second order, $r^{1+w} - r - w(r - 1) = e^{-(1+w)h} - (1+w)e^{-h} + w = \frac{1}{2}w(w + 1)h^2 + O(h^3)$. \square

Proof of Proposition 3. On an eigen-coordinate, $D_c = (1 - A)\xi$, $x - D_c = A\xi$, and $D_u - D_c = (A - B)\xi$; substituting into (15) gives the first expression in (17), and regrouping $1 - A + rA - r(A - B) + r^{1+w}(A - B)$ gives the second. Nonnegativity of each term is $0 \leq B \leq A \leq 1$ and $0 < r < 1$. The regime values and the $r \rightarrow 0$ limit are read off termwise. \square

Proof of Lemma 2. On shared normals $(A, B) = (1, 1)$ one has $D_u - D_c = 0$, so every scalar coefficient gives the DDIM factor r . On tangent directions $(A, B) = (0, 0)$, both denoisers equal the state and every coefficient gives factor 1. On a pure discriminative normal $(A, B) = (1, 0)$, the factor of the scalar update is $r + \alpha(r, w)$. Exactness requires $r + \alpha(r, w) = r^{1+w}$, hence the displayed coefficient, uniquely. \square

Proof of Proposition 4. For $a = 0$, $A \equiv 1$ and $q = 1 - B$. The decomposition (17) gives the coordinate factor

$$G_{\text{fit}} = r_n B_n + r_n^{1+w}(1 - B_n) = r_n [(1 - q_n) + r_n^w q_n].$$

Since $\eta_w = \mu(\sigma)\xi/\sigma$, the residual ratio is $(\mu_{n+1}/\mu_n)(G_{\text{fit}}/r_n)$, which is (18). The bracket is at most 1 because $0 \leq q_n \leq 1$ and $0 < r_n^w \leq 1$, so products telescope:

$$\prod_{n=0}^{k-1} \frac{|\eta_w(\xi_{n+1}, \sigma_{n+1})|}{|\eta_w(\xi_n, \sigma_n)|} \leq \prod_{n=0}^{k-1} \frac{\mu_{n+1}}{\mu_n} = \frac{\mu_k}{\mu_0} \leq 1 + w.$$

□

Theorem 2 (first-order guided AP on the discriminative crossover). *On a discriminative Gaussian coordinate ($a = 0 < b$), for $w \geq 0$ and a uniform λ -mesh of step $0 < h \leq 1$, the fitted step (15) and the exact guided flow satisfy $\xi_K^{\text{fit}} = \Theta_K \xi_K^{\text{ex}}$ with $0 \leq \log \Theta_K \leq \frac{1+h}{4} w(w+2)h$, hence $W_2(\text{Law}(\xi_K^{\text{fit}}), \text{Law}(\xi_K^{\text{ex}})) \leq (e^{w(w+2)h/2} - 1)(\mathbb{E}|\xi_0|^2)^{1/2}$. The multiplier bound and its prefactor are independent of b , K , and σ_{\min} (the W_2 scale carries the initial second moment $(\mathbb{E}|\xi_0|^2)^{1/2}$): on this crossover the fitted step is first-order uniformly accurate against the exact flow’s own pushforward, though the $O(w^2)$ prefactor is not uniform in w .*

Proof. On $a = 0$ the exact one-step factor (Lemma 1) is $\Phi_n = r^{1+w}((1+u_n)/(1+r^2u_n))^{w/2}$, with $u_n = \sigma_n^2/b$, $r = e^{-h}$; the fitted factor (Proposition 3, $A = 1$) is $G_n = e^{-h}(u_n + e^{-wh})/(1+u_n)$. Writing $y_n = \log u_n$, $\delta(h, y) := \log(G_n/\Phi_n) = wh + \log(e^y + e^{-wh}) - (1 + \frac{w}{2}) \log(1 + e^y) + \frac{w}{2} \log(1 + e^{y-2h})$. Then $\delta(0, y) = \partial_h \delta(0, y) = 0$ (first-order consistency, Proposition 2), and with $F(y) = e^y/(1 + e^y)^2$ one has $\partial_h^2 \delta = w^2 F(y + wh) + 2wF(y - 2h) \geq 0$; hence $\delta \geq 0$, so $\Theta_K = \prod_n e^{\delta(h, y_n)} \geq 1$, and Taylor’s formula gives $\delta(h, y_n) = \int_0^h (h-s)[w^2 F(y_n + ws) + 2wF(y_n - 2s)] ds$. On the uniform mesh $y_{n+1} = y_n - 2h$; since $\int F = 1$ and $\text{TV}(F) = \frac{1}{2}$, the rectangle bound gives $2h \sum_n F(y_n + c) \leq 1 + h$ for every shift c , so $\log \Theta_K \leq \int_0^h (h-s) \frac{1+h}{2h} (w^2 + 2w) ds = \frac{1+h}{4} w(w+2)h$. Synchronous coupling with $|\xi_K^{\text{ex}}| \leq |\xi_0|$ (the exact discriminative factor contracts) gives the W_2 bound. □

B THE REVERSE ORDERING

This appendix expands Remark 4.

If a reversed singular direction has $b = 0 < a$ —the marginal collapsed where the class has not—then the exponent (4) tends to $-w$, negative for every $w > 0$: the guided flow itself expands the coordinate as $\sigma \rightarrow 0$, so no discretization can be uniformly stable because the continuous target is not. More generally, reverse ordering with $0 < b < a$ can create finite- σ expansion windows, but only the reversed singular case creates this terminal instability. This is a property of the guidance target, not of the solver; the class-subset hypothesis excludes it by assumption, and autoguidance-style constructions aim to enforce the same directionality.

C METRIC-SPLIT DIAGNOSTICS

To interpret the FID/KID split at the hard cell, we computed post-hoc feature-manifold and sharpness diagnostics on the same images. Fitted CFG improves Inception precision/recall over CFG in both 5k blocks (e.g. 0.799/0.474 versus 0.704/0.360); interval has higher recall but lower precision. The pixel-saturation median is 0.16 for CFG and 0 for fitted CFG and interval, and the median Laplacian energy drops by an order of magnitude—consistent with the fitted step removing oversaturated high-frequency artifacts (we use the Laplacian only as an oversaturation proxy, not as evidence of sharpness). The DINOv2 audit below is a backbone-swapped control on the same split.

Table 3: Tuned vs. terminal limited-interval baselines (5k images per cell). “tuned int.” is the conditionality-selected interval; “terminal int.” is the parameter-free terminal cutoff of Section 4. amp p95 is the 95th-percentile residual amplification, clip p95 the final-denoise clipping fraction, target acc the classifier-proxy target-label accuracy (%).

cell	scheme	FID ↓	KID ↓	amp p95 ↓	clip p95 ↓	target acc ↑
$w=8, N=8$	CFG	32.21	0.0105	13.31	0.575	95.5
	fitted	25.70	0.0180	1.66	0	94.9
	tuned int.	34.25	0.0205	1.71	0.018	95.3
	terminal int.	26.68	0.0225	1.63	0	89.1
$w=8, N=16$	CFG	30.83	0.0117	7.30	0.664	93.8
	fitted	17.12	0.0070	1.66	0.006	99.3
	tuned int.	30.18	0.0120	1.75	0.257	98.8
	terminal int.	12.63	0.0072	1.66	0.000	94.8
$w=6.5, N=8$	CFG	25.36	0.0057	8.08	0.394	98.4
	fitted	25.36	0.0175	1.40	0	94.8
	tuned int.	32.60	0.0208	1.43	0.002	94.7
	terminal int.	26.57	0.0216	1.38	0	89.8

D DINOv2 FEATURE AUDIT

To test whether the FID/KID split is Inception-specific, we recompute feature-space distances with a DINOv2 backbone (dinov2_vits14, CLS-token features; images bilinearly resized to 224) against 50k CIFAR-10 training images. We report the Fréchet distance FD-DINOv2 and an unbiased RBF-kernel MMD (median-heuristic bandwidth, 100 subsets of size 1000). On the two 5k hard-cell blocks, FD-DINOv2 for CFG/fitted/interval is 469.73/230.00/257.88 and 469.10/227.86/254.25, and the DINO-MMD is 0.0258/0.0126/0.0168 and 0.0257/0.0125/0.0164; both favor fitted CFG in both blocks. FD-DINOv2 is the clean backbone-only control; the MMD changes both backbone and kernel relative to Inception KID, so it is corroborating, not a direct KID analogue.

E TUNED LIMITED-INTERVAL BASELINES

The Section 4 interval baseline is the parameter-free terminal cutoff, which on the hard mesh reduces to unguided conditional DDIM. To test whether a *tuned* interval that preserves conditionality can match the fitted step, we selected per cell the conditionality-viable guidance interval $[\sigma_{lo}, \sigma_{hi}]$ from a nine-candidate grid (the one whose target accuracy stays closest to CFG), then scored it on a fresh 5k block. Table 3 reports CFG, the fitted step, the tuned interval, and the terminal interval. In the tested cells, a conditionality-preserving tuned interval does not beat the fitted step on FID; the terminal interval can win FID in a cell ($w=8, N=16$: 12.63 vs 17.12) but pays a clear target-accuracy cost. The fitted step gives interval-like residual stabilization while keeping the guided update active. (Target accuracy is a classifier proxy; the high fitted value at $N=16$ should not be read as fuller conditional fidelity, as it may partly reflect reduced diversity.)

F LATENT-DIFFUSION TRANSFER SMOKE (STABLE DIFFUSION 1.5)

As a cross-domain check that the coefficient is not specific to pixel-space CIFAR EDM, we ran a small Stable Diffusion 1.5 DDIM smoke test at high guidance, swapping only the terminal guidance coefficient. We report pixel saturation (95th percentile of the clipped-pixel fraction) and CLIP image–text alignment; the interval baseline is terminal guidance shutdown. Table 4 shows the fitted step sharply reduces saturation while preserving CLIP alignment far better than shutdown—the same saturation-repair pattern as on CIFAR. This is a smoke/deepen test, not a Stable Diffusion benchmark.

Setup. We use runwayml/stable-diffusion-v1-5 at 512×512 with deterministic DDIM ($\eta = 0$, ϵ -prediction) and float16, over a fixed list of everyday-scene captions (repeated to 256 and 128 prompts) with no negative prompt and seeds matched across schemes. The fitted step

swaps only the terminal guidance coefficient; the interval baseline disables the guidance correction on the terminal steps below the same h_v -derived cutoff. Saturation p95 is the 95th percentile over images of the fraction of final RGB pixels at the valid-range extremes; CLIP alignment uses `openai/clip-vit-base-patch32`.

Table 4: Stable Diffusion 1.5 DDIM smoke test. Saturation p95 (lower is less oversaturated); CLIP mean (higher is better text alignment). “interval” is terminal guidance shutdown.

setting	scheme	saturation p95 ↓	CLIP mean ↑
$g=12, N=12$ (256 img)	CFG	0.134	0.320
	fitted	0.009	0.314
	interval	0.001	0.271
$g=7.5, N=20$ (128 img)	CFG	0.098	0.321
	fitted	0.028	0.319
	interval	0.005	0.278

G ALL-CLASS RESIDUAL AUDIT

The real-checkpoint residual diagnostic (Table 1) uses class 0 and class 1 blocks. To rule out class cherry-picking, we extended it to all ten CIFAR-10 classes on the high-guidance cells ($w \in \{6.5, 8\}$, $N \in \{8, 16, 32\}$; 60 class–cell pairs, all fixed before the run). Clipping/saturation is non-increased in 60/60 pairs, and amp p95 improves in 54/60; the other six are modestly worse on the amp tail (ratios 1.02–1.25, largest class 4 at $w=6.5, N=8$), with clipping still non-increased there. We describe this as *global saturation robustness* and *near-global residual-tail improvement*, and leave the raw counts for the reader to weigh.

H DENSE GUIDED-FLOW REFERENCE

Theorem 2 is an accuracy statement against the exact guided flow’s own pushforward on the calibration model. On learned checkpoints this does *not* extend to final-image accuracy: measured against a 512-step vanilla-CFG reference trajectory, the fitted step is *not* uniformly closer in final denoised-image L_2 (Table 5, ratios > 1), even though its residual and amp tails are far smaller (ratios $\ll 1$). So the learned-checkpoint evidence supports terminal residual/saturation repair, not a claim that the fitted step is a uniformly better coarse integrator of the vanilla CFG field.

Table 5: Dense-reference diagnostic: fitted-CFG/CFG ratios against a 512-step vanilla-CFG reference (512 samples per cell). Final-image rel- L_2 ratios exceed 1 (not closer to the dense CFG endpoint); residual rel- L_2 and amp p95 ratios are far below 1.

cell	image rel- L_2 med	image rel- L_2 p95	residual rel- L_2 p95	amp p95
$w=8, N=8$	1.143	1.109	0.329	0.124
$w=8, N=16$	1.332	1.170	0.884	0.233